KSME

Springer

Journal of Mechanical Science and Technology 36 (8) 2022

Original Article
DOI 10.1007/s12206-022-0725-2

Keywords:
· Cam profile
· Contact stress
· Dual-concave faces
· Instant center

Correspondence to:
Kuan-Lun Hsu
kuanlunhsu@ntu.edu.tw

Citation:
Chuang, Y.-H., Hsu, K.-L., Chang, W.-T. (2022). Design of disk cam mechanisms with a translating follower having symmetrical double-concave faces. Journal of Mechanical Science and Technology 36 (8) (2022) 4043~4052.
http://doi.org/10.1007/s12206-022-0725-2

Received July 22nd, 2021
Revised March 22nd, 2022
Accepted April 4th, 2022

† Recommended by Editor Hyun-Gyu Kim

Design of disk cam mechanisms with a translating follower having symmetrical double-concave faces

Yu-Hsuan Chuang[1], Kuan-Lun Hsu[1] and Wen-Tung Chang[2]

[1]Department of Mechanical Engineering, National Taiwan University, Taipei 10617, Taiwan, [2]Department of Mechanical and Mechatronic Engineering, National Taiwan Ocean University, Keelung 20224, Taiwan

Abstract This paper presents an analytical approach for designing disk cam mechanisms with an improved translating follower having symmetrical double-concave faces. The double-concave faces of such a follower can increase the actual contact area between the cam and the follower. Additionally, during the dwell periods of the follower motion, both the concave faces of the follower can simultaneously contact the cam profile so as to share the carried loading. Such beneficial characteristics can result in a lower level of contact stress between the cam and the follower. Numerical examples are provided to illustrate the nature and the advantage of this improved follower.

1. Introduction

Cam mechanisms have been widely implemented in modern industrial applications, such as automatic tool changers (ATC), internal combustion engines, and pick-and-place devices [1], because they can transform an ordinary motion (either rotation or translation) into a wide variety of intricate output motions simply and efficiently. However, due to the presence of higher pairs in the cam mechanism, the lifetime and the reliability of the cam mechanism [2] is strictly limited, because a higher degree of wear is induced at the interface between the cam and follower surfaces. In real applications, cam wear may deteriorate the performance of the machine. For example, in an internal combustion engine, the wear of the cam can lead to an undesired change in the cam shape and the follower motion program. When the follower displacement declines, hydraulic resistance may consequently increase. Additionally, because of the change in motion program of the follower, the loadings on the links are likely to increase, which may result in damage to the mechanism [3]. Therefore, to reduce the wear rate of the cam surface has been one of the important topics in the product design of cam mechanisms.

Surface fatigue is highly associated with excessive and repeated loadings exposed to the cam profile. For the commonly used type of force-closed cam mechanism [4], one source of external loading results from the spring force which is needed to keep the follower in contact with the cam. To avoid the loss of contact due to the larger inertia force exerted on the follower, it is necessary to increase the retaining force by using a spring with a higher spring rate. However, a higher spring rate contributes more external loading exerted to the follower as well. Especially, the spring reaches its maximum compression and causes the maximum retaining force when the follower is at its highest position (i.e., at its high dwell position). A considerable amount of contact stresses will be induced at the interfaces between the cam and the follower during this period, and such high contact stresses will more likely result in early failure of the cam surface and poor positioning accuracy of the follower in its critical extreme position [4].

In view of the negative effect caused by the higher rate spring, Wu et al. [5] propose a translating follower that has symmetrical double rollers to reduce the pressure angle of the cam mechanism on both the rising and the falling motions of the follower. Besides, both rollers can simultaneously contact the cam profile during the follower's dwell periods so that the carried

load can be evenly shared through both rollers. The effect of the load-sharing is more favorable as the follower dwells at its highest position, where the spring provides the maximum retaining force because of the maximum compression.

The modified follower [5], which provides a two-point contact, can be beneficial to reduce the contact stress between the cam and the follower. However, since profiles of both rollers and the cam are all convex, the actual area of contact is typically very small due to the convex-convex contact. That may still cause an extreme contact stress. Consequently, this article proposes an analytical approach for designing a disk cam mechanism with an improved translating follower that has symmetrical double-concave faces. Because the double-concave faces of such a follower can increase the actual contact area from a practical viewpoint, the contact stress between the cam and the follower can be correspondingly lowered. In addition, during the follower's dwell periods there are two contact points between the cam and the follower surfaces. The carried load can be shared by the symmetrical double-concave faces of the follower, thus the contact force and the contact stress at the interface between the cam and the follower can be reduced as well. These phenomena will be demonstrated through numerical examples to fully disclose the merit of the modified follower.

2. Description of the mechanism

Fig. 1 shows a disk cam mechanism with a translating follower that has symmetrical double-concave faces S_1 and S_2. The dual concave faces, which have the identical radius of the follower curvature, are symmetrically mounted on opposite sides of the centerline of the follower. That is, these dual concave faces have the same value for offset amount e to the left and right. Centers of the follower curvature, C_1 and C_2, are on the right and left sides of the stem centerline of the follower, respectively. The cam is assumed to rotate clockwise, and its profile can be divided into four segments. Segment P_1P_2 is used to drive the follower rises *h* when the cam rotates an angular displacement named β_r. Segments P_2P_3 and P_0P_1, which are circular arcs, are used to produce a high dwell motion when the cam rotates an angular displacement named β_h and a low dwell motion when the cam rotates an angular displacement named β_l, respectively. Segment P_3P_0 is used to drive the follower falls *h* when the cam rotates an angular displacement named β_f. (Angular subscripts *r*, *h*, *f*, and *l* denote rise, high dwell, fall, and low dwell, respectively.) A return spring, which is not shown in the figure, is used to provide a retaining force, therefore the cam maintains contact with at least one of the concave faces during the motion of the follower. Besides, since the cam profile contains the segments of circular arcs that are used to hold the follower stationary, the dual concave faces of the follower will contact the cam simultaneously if each circular arc is large enough to accommodate the span of symmetrical double-concave faces. These contact conditions are explained in detail in the Sec. 4.

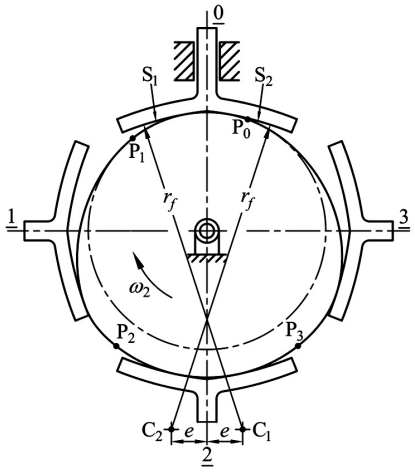

Fig. 1. Disk cam mechanism with a translating follower having symmetrical double-concave faces.

In reference to Fig. 1 at station 0, when the follower is at its lowest position and the velocity of the follower is zero, the concave faces of the follower both contact the cam profile tangentially. At station 1, when the follower has risen above its initial position, only follower face S_1 contacts the cam profile because the radial coordinate of the cam profile is monotonically increasing. During the high dwell period of the follower motion, as shown at station 2, the dual concave faces simultaneously contact the cam profile again. Then, throughout the falling period of the follower motion, since the radial coordinate of the cam profile is monotonically decreasing, only follower face S_2 contacts the cam profile as shown at station 3. Finally, during the low dwell period of the follower motion, the dual concave faces simultaneously contact the cam again, as shown at station 0. It is worth noting that during the dwell periods of the follower motion, the cam simultaneously contacts the dual concave faces of the follower, the carried load on the translating follower can be shared by both concave faces because of the symmetrical arrangement of them. Therefore, the normal contact forces exerted between the cam and the follower correspondingly will be evenly distributed. In addition, the double-concave faces can increase the actual contact area between the cam and the follower from a practical viewpoint. For these reasons, the maximum values of contact stresses can be appreciably reduced at certain phase of the follower motion through the application of this improved follower.

3. Cam profile determination

The analytical approach for determining the entire cam profile, composed of the four segments as shown in Fig. 1, is presented in this section.

3.1 Cam profile for the rising motion of the follower

Fig. 2 shows the disk cam mechanism at a certain phase

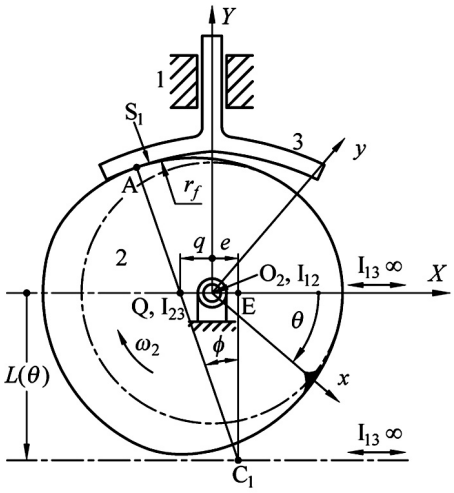

Fig. 2. Disk cam mechanism at a certain phase during the rise of the follower.

during the rising period of the follower motion. When the follower rises, only left concave face S_1 is in contact with the cam profile. The cam profile can be analytically determined by employing the concept of velocity instant centers [6]. For simplicity, the links are numbered as follows: the ground link is designated as link 1, the cam as 2, and the follower as 3. All velocity instant centers, I_{12}, I_{13}, and I_{23}, are located and labeled in the figure. By setting up a Cartesian coordinate system *x*-*y* embedded in the cam and with its origin at fixed pivot O_2, the cam profile coordinates may be expressed in terms of cam rotation angle θ, which is measured against the direction of the cam rotation from body-fixed *x*-axis to *X*-axis of world coordinate *X*-*Y* shown in Fig. 2.

As shown in Fig. 2, by labeling instant center I_{23} as Q and $\boldsymbol{O_2Q} = q$, the speed of point Q on the cam can be expressed as:

$$V_Q = q\omega_2 \tag{1}$$

where ω_2 is the angular velocity of the cam. On the other hand, for a translating follower, all points on the follower have the same velocity. Thus, the speed of point Q on the follower can be expressed as

$$V_Q = \frac{\mathrm{d}L(\theta)}{\mathrm{d}t} = \frac{\mathrm{d}L(\theta)}{\mathrm{d}\theta}\frac{\mathrm{d}\theta}{\mathrm{d}t} = \frac{\mathrm{d}L(\theta)}{\mathrm{d}\theta}\omega_2 \tag{2}$$

where $L(\theta)$ is the position function of the follower:

$$L(\theta) = \sqrt{\left(r_f + r_b\right)^2 - e^2} - S(\theta) \tag{3}$$

where r_b is the radius of the base circle, r_f is the radius of the follower face, which is a negative value for its concave shape, and $S(\theta)$ is the follower displacement program. For a dual-concave-faced follower, the absolute value of r_f is much larger than those of r_b and $S(\theta)$. Instant center I_{23} (point Q) is a point common to the links 2 (cam) and 3 (follower) that have the same velocity. Thus, from Eqs. (1) and (2),

$$q = \frac{\mathrm{d}L(\theta)}{\mathrm{d}\theta} = \frac{\mathrm{d}S(\theta)}{\mathrm{d}\theta} = V(\theta) \tag{4}$$

where $V(\theta)$ is the follower velocity program. During the rising period of the follower motion, the value of $V(\theta)$ remains positive. Once r_b, r_f and $S(\theta)$ have been selected, for each specified value of θ, center C_1 of the left concave face can be located by applying Eq. (3), and point Q can be located by applying Eq. (4).

The pressure angle [4] is defined as the angle between the common normal, as known as the direction of the reaction force at the contact point, and the direction of motion of the follower. For the pressure angle at contact point A, it is the angle between common normal $\boldsymbol{C_1A}$ and velocity direction $\boldsymbol{C_1E}$. From triangle QC_1E, pressure angle ϕ can be expressed as:

$$\phi = \tan^{-1}\left[\frac{q+e}{L(\theta)}\right] = \tan^{-1}\left[\frac{V(\theta)+e}{L(\theta)}\right], \tag{5}$$

in which e is always positive.

Therefore, the vector equation for the profile coordinates of contact point A can be expressed as

$$\boldsymbol{O_2A} = \boldsymbol{O_2E} + \boldsymbol{EC_1} + \boldsymbol{C_1A}\ . \tag{6}$$

In world coordinate *X*-*Y*, the three vectors at the right side of Eq. (6) are

$$\boldsymbol{O_2E} = e\boldsymbol{I}\ , \tag{7}$$

$$\boldsymbol{EC_1} = -L(\theta)\boldsymbol{J}\ , \tag{8}$$

$$\boldsymbol{C_1A} = r_f\sin\phi\,\boldsymbol{I} - r_f\cos\phi\,\boldsymbol{J}\ . \tag{9}$$

Therefore, the parametric equations for the coordinates of contact point A on the cam profile for the upward motion are

$$\boldsymbol{O_2A} = \left(e + r_f\sin\phi\right)\boldsymbol{I} + \left(-L(\theta) - r_f\cos\phi\right)\boldsymbol{J}\ . \tag{10}$$

The angle between *x*-axis of the body-fixed coordinate and *Y*-axis of the world coordinate is θ and against the rotation direction of the cam. Thus, a rotation matrix, denoted by Eq. (11), is adopted to obtain the coordinate of the point on the body-fixed coordinate:

$$\begin{bmatrix} \mathrm{x} \\ \mathrm{y} \end{bmatrix} = \begin{bmatrix} \cos\theta & -\sin\theta \\ \sin\theta & \cos\theta \end{bmatrix}\begin{bmatrix} \mathrm{X} \\ \mathrm{Y} \end{bmatrix}. \tag{11}$$

Therefore, the coordinates of $\boldsymbol{O_2A}$ in *x*-*y* system in terms of

the body-fixed coordinate can be expressed as

$$\boldsymbol{O_2A} = \left(L(\theta)\sin\theta + e\cos\theta + r_f \sin\left(\phi+\theta\right)\right)\boldsymbol{i} + \left(-L(\theta)\cos\theta + e\sin\theta - r_f\cos(\phi+\theta)\right)\boldsymbol{j}. \quad (12)$$

3.2 Cam profile for the falling motion of the follower

Fig. 3 shows the disk cam mechanism at a certain phase during the falling period of the follower motion. When the follower falls, only the right concave face S_2 is in contact with the cam profile. Similarly, the cam profile can be determined by employing the concept of velocity instant centers [6].

At this stage, the follower has a downward motion and thus follower velocity program $V(\theta)$ becomes negative while the value of e remains positive. Therefore, from triangle QC_2E, pressure angle ϕ at the contact point B can be expressed as:

$$\phi = \tan^{-1}\left[\frac{e-q}{L(\theta)}\right], \quad (13)$$

in which ϕ remains positive.

Therefore, the vector equation for the profile coordinates of contact point B can be expressed as

$$\boldsymbol{O_2B} = \boldsymbol{O_2E} + \boldsymbol{EC_2} + \boldsymbol{C_2B} \quad (14)$$

where

$$\boldsymbol{O_2E} = -e\,\boldsymbol{I}, \quad (15)$$

$$\boldsymbol{EC_2} = -L(\theta)\boldsymbol{J}, \quad (16)$$

$$\boldsymbol{C_2B} = -r_f\sin\phi\,\boldsymbol{I} - r_f\cos\phi\,\boldsymbol{J}. \quad (17)$$

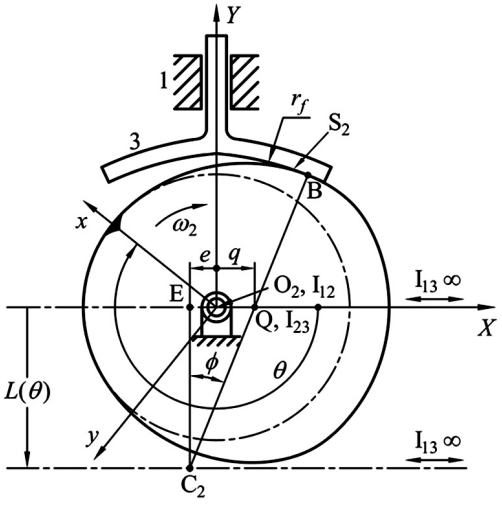

Fig. 3. Disk cam mechanism at a certain phase during the fall of the follower.

Therefore, the parametric equations for the coordinates of contact point B on the cam profile for the downward motion are

$$\boldsymbol{O_2B} = \left(-e - r_f\sin\phi\right)\boldsymbol{I} + \left(-L(\theta) - r_f\cos\phi\right)\boldsymbol{J}. \quad (18)$$

Similarly, the rotation matrix given in Eq. (11) is adopted to project the coordinates of the cam profile described in world coordinate, onto *x*-*y* plane. Thus, the coordinates of $\boldsymbol{O_2B}$ can be expressed as

$$\boldsymbol{O_2B} = \left(L(\theta)\sin\theta - e\cos\theta - r_f\sin\left(\phi-\theta\right)\right)\boldsymbol{i} + \left(-L(\theta)\cos\theta - e\sin\theta - r_f\cos(\phi-\theta)\right)\boldsymbol{j}. \quad (19)$$

3.3 Cam profile for the dwell motions of the follower

For the low dwell period of the follower motion, the radius of the circular cam segment is r_b, which is the radius of base circle. For the high dwell motion, the circular cam segment must have a radius of R, which is determined by

$$R = \left|r_f\right| - \sqrt{\left(r_f + r_b\right)^2 - 2h\sqrt{\left(r_f + r_b\right)^2 - e^2} + h^2} \quad (20)$$

where h is the total lift of the follower motion. Note that two identical concave faces of the follower must have equal offset amount e, so that both circular cam segments are able to simultaneously contact both concave faces of the follower.

3.4 Radius of curvature of the cam profile

Since the cam profile can be expressed in the form of the parametric equations of $x = x(\theta)$ and $y = y(\theta)$, its radius of curvature [7] can be expressed as

$$\rho = \frac{\{[x'(\theta)]^2 + [y'(\theta)]^2\}^{1.5}}{x'(\theta)y''(\theta) - x''(\theta)y'(\theta)} \quad (21)$$

where the prime denotes differentiation with respect to θ. From Eq. (21), the radius of curvature of the cam profile can then be determined by substituting *x*- and *y*-component of Eqs. (12) and (19) into Eq. (21). To prevent unintended multiple-point or non-contact point conditions, the radius of curvature of the cam profile must not exceed that of the follower. Therefore, the following restrictive condition must be satisfied:

$$0 < \rho(\theta) < |r_f|. \quad (22)$$

This relation also indicates that the cam profile must always be convex.

4. Geometric design limitations

In addition to the equal offset amount e for the two identical

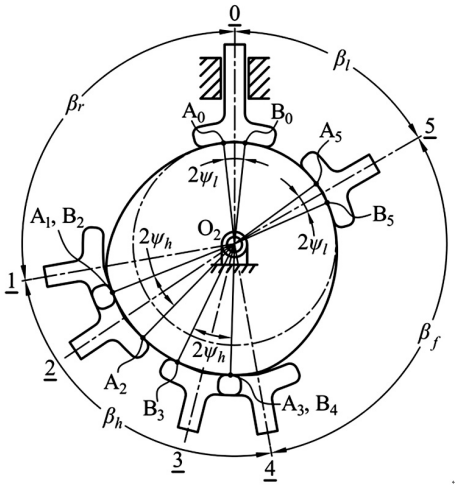

Fig. 4. Cam profile with circular segments that can accommodate the span of symmetrical double-concave faces.

concave faces of the follower, the cam mechanism has other geometric design limitations as well. To result in a smooth contact transition of the follower faces, each segment of the circular cam profile must be large enough. Fig. 4 shows a typical double-dwell cam profile as well as the follower at its various stations. While the cam rotates clockwise, the cam profile is used to drive the follower rises a total lift of h for a cam rotation angle of β_r, produces high dwell for the next cam rotation angle of β_h, falls h for a cam rotation angle of β_f, and produces low dwell for the remaining cam rotation angle of β_l. At station 0 shown in Fig. 4, when the cam rotation angle θ = 0°, the follower is at its lowest position and the velocity of the follower is zero. The two concave faces of the follower both contact the cam profile tangentially at points A_0 and B_0, respectively, and $O_2A_0 = O_2B_0 = r_b$. Here, the subscript 0 of points A_0 and B_0 denotes the station number 0. After the cam rotates clockwise from θ = 0° to $\theta = \beta_r$, the follower occupies station 1 and is at its highest position. Notice that for $0 \le \theta \le \beta_r$ only concave face S_1 is in contact with the cam. At this station, concave face S_1 contacts the cam profile at point A_1, which is the beginning point of the circular profile segment for the high dwell and $O_2A_1 = R$, the maximum radial dimension of the cam profile.

When the cam rotates clockwise to $\theta = \beta_r + 2\psi_h$, the follower occupies station 2. The concave faces S_1 and S_2 simultaneously contact the cam profile at points A_2 and B_2, respectively. At this instant, since point A_1 is at the first instant that the follower reaches the highest position, point B_2 must coincide with A_1. From geometry, half the subtending angle of $\angle A_2O_2B_2$, which can be expressed as

$$\psi_h = \sin^{-1}\left(\frac{e}{-R - r_f}\right). \tag{23}$$

This is the beginning of the phase in which both concave faces simultaneously contact the cam profile during the high dwell period. From now on, the carried load is wholly balanced by the symmetrical double-concave faces of the follower.

When the cam rotates clockwise to $\theta = \beta_r + \beta_h + 2\psi_h$ (i.e., at station 3) both concave faces still contact the cam profile simultaneously, and concave face S_1 contacts the cam profile at point A_3. This is the end of the phase in which both concave faces simultaneously contact the cam profile during the high dwell period, and point A_3 is the end point of this circular profile segment. From geometry, segment A_1A_3 is the circular cam profile for the follower high dwell, and its subtending angle is

$$\angle A_1O_2A_3 = \beta_h - 2\psi_h. \tag{24}$$

In the next consecutive cam rotation angle, the concave face S_1 will lose its contact with the cam profile, but the follower still remains stationary and is at its highest position.

When the cam rotates clockwise to $\theta = \beta_r + \beta_h$ (i.e., at station 4), the concave face S_2 reaches the previous location of the concave face S_1, and the concave face S_2 contacts the cam profile at point B_4, which is coincident with the point A_3. This is the beginning of the phase in which the follower falls, and the concave face S_2 is adopted for the determination of the cam profile.

At station 5, When the cam rotates clockwise to $\theta = \beta_r + \beta_h + \beta_f$ (i.e., at station 5), the end of the phase in which the follower falls, the follower returns to the lowest position and remains stationary until θ = 360° to complete the motion cycle. This station is also the end of the phase in which concave face S_2 is the effective role to determine the cam profile. Here, concave faces S_1 and S_2 simultaneously contact the cam profile at points A_5 and B_5, respectively. From geometry, half the subtending angle of $A_5O_2B_5$, which can be expressed as

$$\psi_l = \sin^{-1}\left(\frac{e}{-r_f - r_b}\right). \tag{25}$$

In addition, segment B_5A_0 is the circular cam profile for the follower low dwell and its subtending angle is

$$\angle B_5O_2A_0 = \beta_t + 2\psi_l. \tag{26}$$

Correspondingly, to accommodate both concave faces during the dwell period of the follower motion, each segment of the circular cam profile must be large enough. For the low dwell portion, $\angle B_5O_2A_0$ must be greater than $2\psi_l$, which means

$$\beta_l \ge 0. \tag{27}$$

Also, for the high dwell portion, $\angle A_1O_2A_3$ must be greater than $2\psi_h$, which means

$$\beta_h \ge 4\psi_h. \tag{28}$$

5. Force analysis and contact stress evaluation

To illustrate how the improved follower affects the induced contact stress, it is necessary to calculate the net forces exerted on the follower. For drawing the free-body diagrams, the notations are predefined as follows: d is the guide width or diameter of the follower, l_1 is the overhang length that will vary while the follower is moving, l_2 is the follower guide length, μ is the friction coefficient between the follower stem and its guide. Also, F_1 is a reaction force normal to the lower follower stem, F_2 is another reaction force normal to the upper follower stem, and F_N is the contact force normal to the cam profile. The components of total force F_t acting on the follower including the static effective weight, the spring force, and the inertia force can be expressed as

$$F_t = M\left[g + a(\theta)\right] + ks \tag{29}$$

where M is the effective mass of the follower, g is the gravitational acceleration, $a(\theta) = A(\theta)\omega_2^2$ (For $A(\theta)$ being the follower acceleration program) is the acceleration of the follower, k is the spring constant of the return spring, and s is the total compressed amount of the return spring. Note that Eq. (29) is valid if the follower motion direction is parallel to that of gravity. In reality, the follower could be required to perform a task along a certain direction, which is not aligned with the gravity field. In addition, with limited device layout, not aligning the gravity field with the direction of the follower motion could also be a preferable option. However, to demonstrate the strength of the presented follower without distraction, we intend to simplify the force and contact stress analyses by assuming the follower motion aligning with the gravity field. The total compressed amount of the return spring s consists of its initial compressed amount s_p and the displacement of the follower and can be expressed as

$$s = S(\theta) + s_p \ . \tag{30}$$

Fig. 5 shows the free-body diagram of the double-concave-face follower in the rising period. Notice that during the follower's rising period, the direction of friction forces f_1 and f_2 must always be downward. Because friction forces f_1 and f_2 are always against the direction of the follower motion, the directions of reaction forces F_1 and F_2 might change according to the nature of the friction force.

By using the Coulomb friction law, it can be known that

$$f_1 = \mu F_1 \ , \tag{31}$$

$$f_2 = \mu F_2 \ . \tag{32}$$

While either F_1 or F_2 becomes negative, it means that F_1 or F_2 might be in the reverse direction defined in the free body diagram. Because the signs of frictions f_1 and f_2 follow those of F_1 and F_2, negative values in either F_1 or F_2 result in the upward frictions f_1 and f_2, which violates the nature of the friction force during the follower's rising period. To comprehensively simulate all possible contacting modes for the follower within the sliding guideway under a reasonably close running or sliding fit, four possible situations [8] are taken into account as shown in Fig. 6. Here, the free body diagram in Fig. 6(a) is selected as a demonstrative case for the following force analysis.

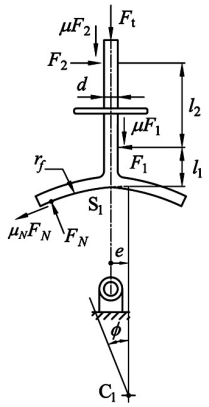

Fig. 5. Free-body diagram of the double-concave-face follower in the rising motion.

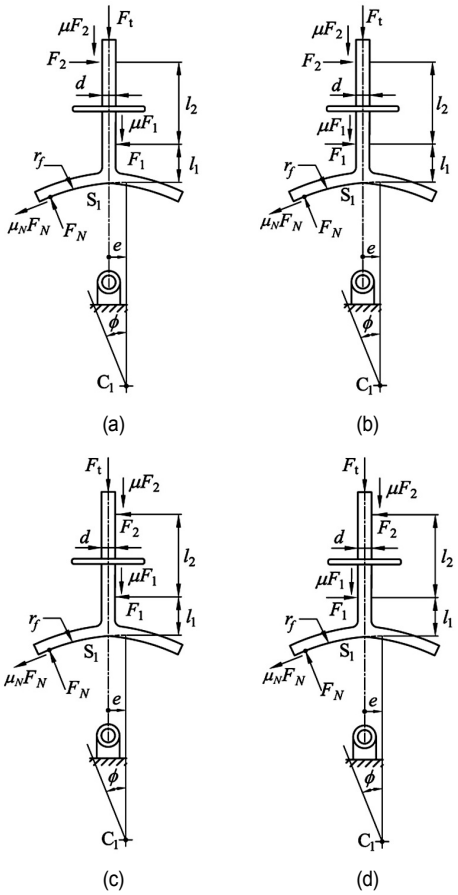

Fig. 6. Four possible contacting situations for the follower configurations relative to the sliding guideway.

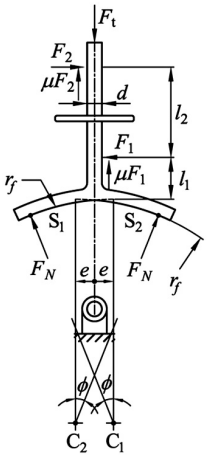

Fig. 7. Free-body diagram of the double-concave-faced follower in the dwelling motio.

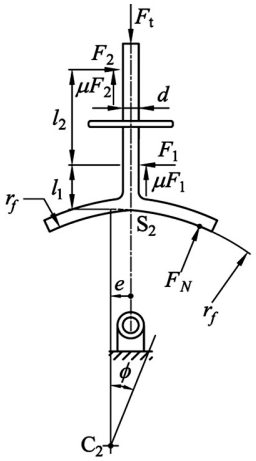

Fig. 8. Free-body diagram of the double-concave-face follower in the falling motion.

The follower is assumed in a state of two-dimensional equilibrium; three equations of equilibrium in such a planar case, which include unknowns F_1, F_2, and F_N acting on the follower, can be expressed as:

$$\sum F_x = -F_1 + F_2 - F_N \sin\phi = 0\,, \tag{33}$$

$$\sum F_y = -F_t - \mu(F_1 + F_2) + F_N \cos\phi = 0\,, \tag{34}$$

$$\sum M_z = F_1(l_1 - r_f) - F_2(l_1 + l_2 - r_f) + \mu F_1\left(e - \frac{d}{2}\right) + \mu F_2\left(e + \frac{d}{2}\right) + F_t e = 0. \tag{35}$$

The aforementioned equations of equilibrium can be solved simultaneously to find the values of unknowns F_1, F_2 and F_N. If reaction force F_1 or F_2 is negative, other free body diagrams in Fig. 6 will be accessed in succession until both F_1 and F_2 are positive, and thus in the right direction as defined in the corresponding free body diagram.

As shown in Fig. 7, in the dwell period of the follower motion, there will be two contact points between the cam and the follower simultaneously. Similarly, three equations of equilibrium can be derived and solved simultaneously to find the values of unknowns F_1, F_2 and F_N:

$$\sum F_x = -F_1 + F_2 = 0\,, \tag{36}$$

$$\sum F_y = -F_t + \mu(F_1 + F_2) + 2F_N \cos\phi = 0\,, \tag{37}$$

$$\sum M_z = F_1 l_1 - F_2(l_1 + l_2) + \mu F_1 \frac{d}{2} - \mu F_2 \frac{d}{2} = 0\,. \tag{38}$$

Due to the symmetry of the follower, the two horizontal components of F_N have the same magnitude but in the opposite direction. On the other hand, the vertical components of F_N are of the same magnitude and in the same direction so that the total force F_t can be evenly distributed.

Fig. 8 shows the free-body diagram for the falling period of the follower motion. In this case, the friction forces point upward against the falling motion. The equilibrium equations for solving the forces are

$$\sum F_x = -F_1 + F_2 + F_N \sin\phi = 0\,, \tag{39}$$

$$\sum F_y = -F_t + \mu(F_1 + F_2) + F_N \cos\phi = 0\,, \tag{40}$$

$$\sum M_z = F_1(l_1 - r_f) - F_2(l_1 + l_2 - r_f) + \mu F_1\left(e + \frac{d}{2}\right) + \mu F_2\left(e - \frac{d}{2}\right) - F_t e = 0. \tag{41}$$

Similarly, if F_1 or F_2 is negative, models which have different contact modes for the follower within the sliding guideway will be accessed until both F_1 and F_2 are positive so that the forces follow the nature of friction.

Once contact force F_N is determined by the aforementioned force analysis, the maximum contact stress between the cam and the follower surfaces, denoted by σ, can be evaluated according to the Hertz contact theory [9]:

$$\sigma = \sqrt{\frac{F_N\left(\frac{1}{r_f} + \frac{1}{\rho}\right)}{\pi w\left[\left(\frac{1-\nu_1^2}{E_1}\right) + \left(\frac{1-\nu_2^2}{E_2}\right)\right]}} \tag{42}$$

where ρ is the radius of curvature of the cam profile corresponding to the contact point between the cam and the follower (referring to Eq. (21)), E_1 and E_2 are, respectively, Young's modulus of elasticity for the cam and the follower, ν_1 and ν_2 are, respectively, Poisson's ratios for the cam and the follower, and w is the width of contact.

6. Examples

To illustrate the advantages of the proposed follower, force

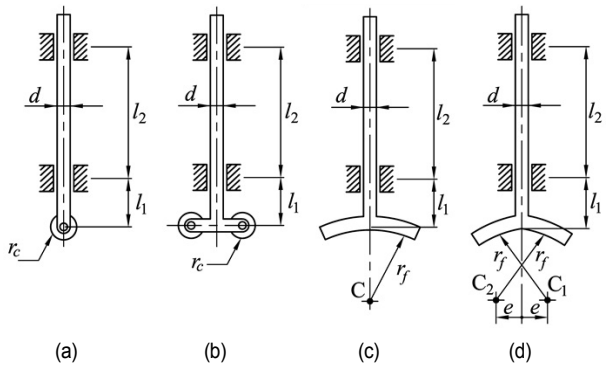

Fig. 9. Four different types of translating followers.

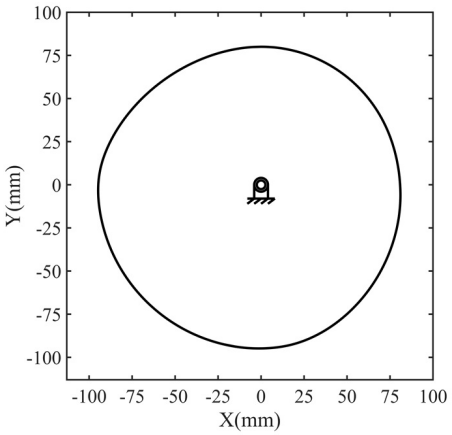

Fig. 10. The profile of the double concave follower cam.

analysis and the contact stress evaluation for four different types of followers (see Fig. 9) were performed, and their results were compared. Fig. 9 shows the four translating followers with a single roller (as Fig. 9(a)), symmetrical double rollers [5] (as Fig. 9(b)), a single concave face [10] (as Fig. 9(c)), and the proposed symmetrical double-concave faces (as Fig. 9(d)), respectively.

In this analysis, a disk cam rotating at 1200 rpm constantly ($\omega_2 \approx 125.66$ rad/s CW) is used to drive its follower to rise 15 mm with a cycloidal motion while the cam rotates clockwise from 0° to 100°, dwell from 100° to 170°, return with a cycloidal motion from 170° to 300°, and dwell for the remaining 60°. The dimensional parameters are: the radius of the base circle r_b is 80 mm, the radii of the rollers r_c are all 8 mm, the radii of the concave-faces r_f are all -250 mm, the offsets e of both the double-roller follower and the double-concave-face follower are 10 mm, and the single-roller follower and the single-concave-face follower are without offsets. The widths w of the cam and the follower are both 15 mm, and the guide width or diameter d of each follower is 8 mm. The guide distance l_2 is 80 mm, the initial value of l_1 is 30 mm, the initial compression of the spring s_p is 5 mm, and the spring constant k is 6772.5 N/m (which is designed based on the method from Refs. [11, 12]). The materials of the cam and the follower are both steel, the friction coefficients are $\mu_N = \mu = 0.1$, Young's moduli are $E_1 = E_2 =$ 210 GPa, Poisson's ratios are $\nu_1 = \nu_2 = 0.29$, and the mass of the follower M is 108 g.

Table 1. Maximum values of the contact force F_N in four types of cam mechanisms during high dwell periods.

Number of rollers or concave faces	Value of $F_{N,max}$ (N)	
	Roller follower	Concave-face follower
Single	133.496	129.161
Double	67.297	67.297

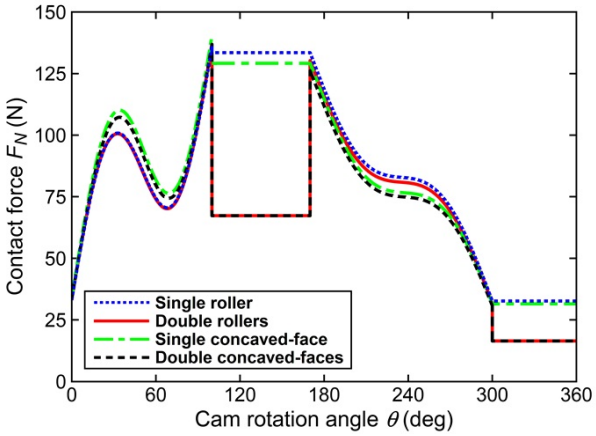

Fig. 11. Contact forces normal to the cam profile of four different followers.

The synthesized cam profile for the double-concave-face follower is illustrated in Fig. 10. (Note that the cam profiles for the other three types of followers are also synthesized but not graphically presented.) The contact forces F_N normal to the cam profiles, with respect to the cam rotating angle θ, are shown in Fig. 11, and the corresponding maximum values of F_N during high dwell periods are listed in Table 1. It can be noticed in Fig. 11 that for the follower with a single roller or with a single concave face, its contact force during the high dwell period is at a relatively high level, since the spring reaches its maximum compression and causes the maximum spring force. For the follower with symmetrical double concave faces, its contact force during the high dwell period is 67.297 N and 52.10 % of that of a follower with a single concave face, which is 129.161 N. Similarly, the maximum of F_N of the follower with symmetrical double rollers (67.297 N) is approximately half (50.41 %) of that of the follower with a single roller (133.496 N). Such high rates of reduction (more than 50 %) contributed by the followers with the symmetrical double rollers and the symmetrical double concave faces are based on that they can generate two contact points during high dwell and distribute the contact forces normal to the cam profile.

Fig. 12 illustrates reaction forces F_1 and F_2 with respect to the cam rotation angle θ, respectively, and their maximum absolute magnitudes are correspondingly listed in Table 2. Notice that the maximum absolute magnitudes of F_1 and F_2 are all smaller than that of F_N. Furthermore, since both F_1 and F_2 are exerted on sliding pairs, which are lower pairs, the caused

Table 2. Maximum absolute magnitudes of F_N, F_1 and F_2 in four types of cam mechanisms.

	Single roller	Double roller	Single concave face	Double concave faces
θ (degree)	99.98	99.98	99.98	99.98
$F_{N,max}$ (N)	135.615	136.838	140.405	136.865
θ (degree)	42.48	170.00	41.82	42.72
$\|F_1\|_{max}$ (N)	15.905	25.097	66.527	52.576
θ (degree)	213.3	170.00	41.94	234.20
$\|F_2\|_{max}$ (N)	2.061	18.055	50.861	41.324

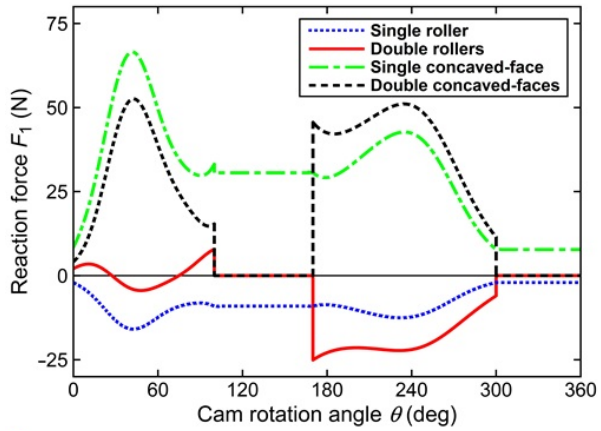

(a)

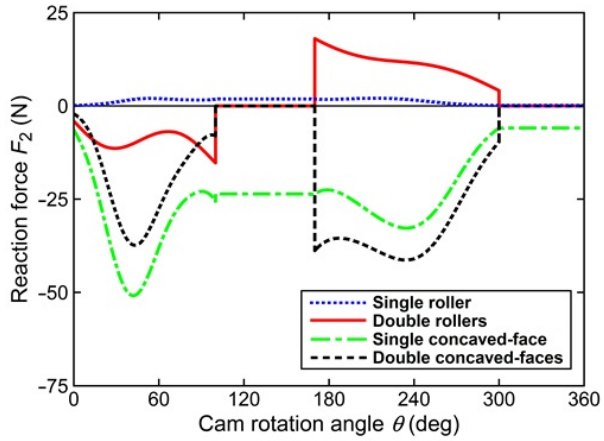

(b)

Fig. 12. Forces normal to the follower stem of four different followers.

wear should be smaller than that caused by F_N. Thus, the forces occurring at the sliding pairs may not be the major concern when designing the proposed type of cam mechanisms.

Fig. 13 illustrates the contact stresses σ with respect to the cam rotation angle θ. Due to the larger contact area, the contact stresses of the concave-faced followers (with their maximum values less than 71 MPa) are all smaller than those of the roller followers (with their maximum values greater than 210 MPa). In addition, the symmetrical double-concave-face follower can cause two-point contact during the dwell periods

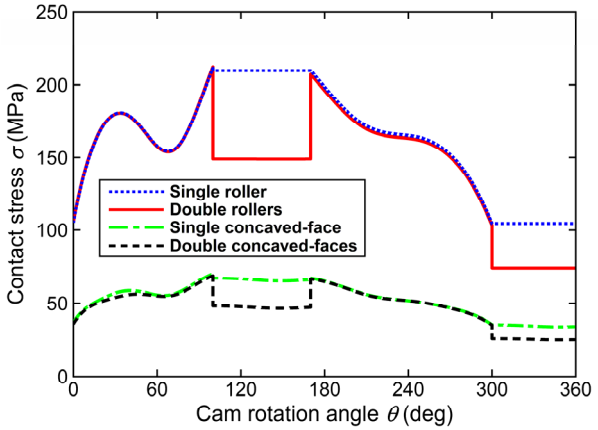

Fig. 13. Contact stresses induced at the surfaces of the cam profile of four different followers.

and distribute the contact forces normal to the cam profile, so it has the smallest contact stress among the four types of follower. The reduced contact stress may result in a lower wear rate of the cam profile during the dwell period, preventing an early failure of the cam surface and maintaining the position accuracy of the follower in its critical extreme position [4].

7. Conclusions

An analytical approach for designing the disk cam mechanism with a translating follower having symmetrical double-concave faces has been proposed. The dual concave faces of such a follower are symmetrically mounted on opposite sides of the centerline of the follower, and they can take turns to contact the cam profile when the cam rotates. From a practical viewpoint, concave faces can effectively increase the actual area of contact. Through the application of the improved follower, there are two contact points between the cam and the follower at a certain phase during the high or low dwell period of the follower. The symmetrical arrangement of concave faces can spread the carried loading by offering two cam-follower pairs. Therefore, the contact forces and the contact stresses can be at lower levels when the both concave faces contact the cam profile simultaneously.

Acknowledgments

Kuan-Lun Hsu would like to express his gratitude to Dr. Long-long Wu, whose enthusiasm for cam mechanisms makes this paper possible. In addition, he also wishes to acknowledge the support of the Department of Mechanical Engineering at National Taiwan University. And he offers his grateful thanks to the dedicated referees of this work, whose collective comments form the fundamentals of the research. Most importantly, the Young Scholar Fellowship Program supported by the Ministry of Science and Technology of Taiwan (MOST 110-2636-E-002 -023 and MOST 111-2222-E-002-002-MY3) encourages him to be fearlessly devoted to his research. At last, Wen-Tung

Chang would like to express his gratitude for the financial support from the Ministry of Science and Technology of Taiwan under grant number MOST-110-2221-E-019-059.

References

[1] W. T. Chang, L. I. Wu and C. H. Liu, The kinematic design of a planar-cam type pick-and-place device, *Journal of Mechanical Science and Technology*, 22 (12) (2008) 2328-2336.
[2] M. Hejnová, Service life assessment of the cam mechanisms, *Procedia Engineering*, 96 (2014) 157-163.
[3] A. Vasilyev, E. Deynichenko and D. Popov, Internal combustion engine valve gear cam wear and its influence on valve gear and engine efficiency, *Mechanics*, 54 (4) (2005) 44-49.
[4] R. L. Norton, *Cam Design and Manufacturing Handbook*, Industrial Press, New York (2002).
[5] L. I. Wu, C. H. Liu, K. L. Shu and S. L. Chou, Disk cam mechanisms with a translating follower having symmetrical double rollers, *Mechanism and Machine Theory*, 44 (11) (2009) 2085-2097.
[6] L. I. Wu, Calculating conjugate cam profiles by vector equations, *Proceedings of the Institution of Mechanical Engineers, Part C: J. of Mechanical Engineering Science*, 217 (10) (2003) 1117-1123.
[7] J. Reeve, *Cams for Industry*, Mechanical Engineering Publications Limited, London (1995).
[8] B. Paul, *Kinematics and Dynamics of Planar Machinery*, Prentice Hall, New Jersey, USA (1979).
[9] J. A. Collins, *Mechanical Design of Machine Elements and Machines*, Wiley, New York (2003).
[10] L. I. Wu, C. H. Liu and T. W. Chen, Disc cam mechanisms with concave- faced followers, *Proceedings of the Institution of Mechanical Engineers, Part C: J. of Mechanical Engineering Science*, 223 (6) (2009) 1443-1448.
[11] R. G. Budynas, J. K. Nisbett and J. E. Shigley, *Shigley's Mechanical Engineering Design*, 10th Ed., McGraw-Hill Education, New York, USA (2015).
[12] J. Volmer, *Getriebetechnik: Kurvengetriebe*, Verl. Technik, Berlin (1976).

Yu-Hsuan Chuang is currently a University Assistant at National Taiwan University, Taipei, Taiwan. Her research interests include cam design and analysis in the mechanism design lab and robot vision in precision system control lab.

Kuan-Lun Hsu is currently an Assistant Professor of Mechanical Engineering at National Taiwan University, Taipei, Taiwan. He holds a dual-degree at the doctoral level in engineering at National Tsing Hua University and Tennessee Technological University. His research interests include kinematics and dynamics of machinery, mechanism and machine design, and cam-follower system.

Wen-Tung Chang is currently an Associate Professor of Mechanical and Mechatronic Engineering at National Taiwan Ocean University in Keelung, Taiwan. He received his Ph.D. in Power Mechanical Engineering from National Tsing Hua University in 2007. His current research interests include kinematics and dynamics of machinery, innovative mechanism and machine design, cam design and manufacture, precision mechanical measurement, and design of automated optical inspection (AOI) systems.